Magnetic-field-influenced nonequilibrium transport through a quantum ring with correlated electrons in a photon cavity

Thorsten Arnold,[1,*] Chi-Shung Tang,[2,†] Andrei Manolescu,[3] and Vidar Gudmundsson[1,‡]
[1]*Science Institute, University of Iceland, Dunhaga 3, IS-107 Reykjavik, Iceland*
[2]*Department of Mechanical Engineering, National United University, 1, Lienda, Miaoli 36003, Taiwan*
[3]*Reykjavik University, School of Science and Engineering, Menntavegur 1, IS-101 Reykjavik, Iceland*
(Received 11 September 2012; revised manuscript received 15 November 2012; published 31 January 2013)

We investigate magnetic-field-influenced time-dependent transport of Coulomb interacting electrons through a two-dimensional quantum ring in an electromagnetic cavity under nonequilibrium conditions described by a time-convolutionless non-Markovian master equation formalism. We take into account the full electromagnetic interaction of electrons and cavity photons. A bias voltage is applied to semi-infinite leads along the x axis, which are connected to the quantum ring. The magnetic field is tunable to manipulate the time-dependent electron transport coupled to a photon field with either x or y polarization. We find that the lead-system-lead current is strongly suppressed by the y-polarized photon field at magnetic field with two flux quanta due to a degeneracy of the many-body energy spectrum of the mostly occupied states. On the other hand, the lead-system-lead current can be significantly enhanced by the y-polarized field at magnetic field with half-integer flux quanta. Furthermore, the y-polarized photon field perturbs the periodicity of the persistent current with the magnetic field and suppresses the magnitude of the persistent current. The spatial and temporal density distributions reflect the characteristics of the many-body spectrum. The vortex formation in the contact areas to the leads influences the charge circulation in the ring.

DOI: 10.1103/PhysRevB.87.035314 PACS number(s): 73.23.−b, 78.67.−n, 85.35.Ds, 73.23.Ra

I. INTRODUCTION

Quantum interference phenomena are essential when developing quantum devices. Quantum confined geometries conceived for such studies may consist of which-path interferometers,[1,2] coupled quantum wires,[3,4] side-coupled quantum dots,[5,6] or quantum rings.[7,8] These coupled quantum systems have captured interest due to their potential applications in electronic spectroscopy tools[9] and quantum information processing.[10] Furthermore, the magnetic flux through the ring system can drive persistent currents[11] and lead to the topological quantum interference phenomenon known as the Aharonov-Bohm (AB) effect.[12–16] Both, the persistent current and ring conductance show characteristic oscillations with period of one flux quantum, $\Phi_0 = hc/e$. The free spectrum of the one-dimensional quantum ring exhibits level crossings at half-integer and integer multiples of Φ_0.[17,18] The persistent current dependence on the magnetic field[19] and electron-electron interaction strength[20] has been investigated adopting a two-dimensional quantum ring model with analytically known noninteracting properties.[21] Varying either the magnetic field or the electrostatic confining potentials allows the quantum interference to be tuned.[22]

There has been considerable interest in the study of electronic transport through a quantum system in a strong system-lead coupling regime driven by periodic time-dependent potentials,[23–26] longitudinally polarized fields,[27–29] or transversely polarized fields.[30,31] On the other hand, quantum transport driven by a transient time-dependent potential enables development of switchable quantum devices, in which the interplay of the electronic system with external perturbation plays an important role.[32–35] These systems are usually operated in the weak system-lead coupling regime and described within the wide-band or the Markovian approximation.[36–38] Within this approximation, the energy dependence of the electron tunneling rate or the memory effect in the system are neglected by assuming that the correlation time of the electrons in the leads is much shorter than the typical response time of the central system. However, the transient transport is intrinsically linked to the coherence and relaxation dynamics and cannot generally be described in the Markovian approximation. The energy-dependent spectral density in the leads has to be included for accurate numerical calculation.

In order to explicitly explore the transport dynamics with the electron-photon coupling and the transient system-lead coupling, a non-Markovian density-matrix formalism involving the energy-dependent coupled elements should be considered based on the generalized master equation (GME).[39–42] How to appropriately describe the carrier dynamics under nonequilibrium conditions with realistic device geometries is a challenging problem.[43,44] More recently, manipulation of electron-photon coupled quantum systems embedded in an electromagnetic cavity has become one of the most promising applications in quantum information processing devices. Utilizing the giant dipole moments of intersubband transitions in quantum wells[45,46] enables researchers to reach the ultrastrong electron-photon coupling regime.[47–49] In this regime, the dynamical electron-photon coupling mechanism has to be explored beyond the wide-band and rotating-wave approximations.[50–52] Nevertheless, time-dependent transport of Coulomb interacting electrons through a topologically nontrivial broad ring geometry in an electromagnetic cavity with quantized photon modes remains unexplored beyond the Markovian approximation.

In the present work, we explore the transient effects of electronic transport through a broad quantum ring in a linearly polarized electromagnetic cavity coupled to electrically biased leads. This electron-photon coupled system under investigation can be manipulated by tuning the applied magnetic field and the polarization of the photon field. A time-convolutionless

(TCL) version of the GME is utilized to project the time evolution onto the central system by taking trace with respect to the operators in the leads.[53–55] We demonstrate the transient transport properties by showing the many-body (MB) energy spectra, the time-dependence of the electric charge, the magnetic-field dependence of the total charge current with (w) or without (w/o) photon cavity, the charge density distribution, the normalized current density distribution and the local current coming from an occupation redistribution of the MB states in the central quantum ring system.

The paper is organized as follows. In Sec. II, the theoretical model is described. The electron system is embedded in an electromagnetic cavity by coupling a many-level electron system with photons using the full photon energy spectrum of a single cavity mode. In Sec. III, we show the numerical results for the dynamical transient transport properties for different magnetic field and photon field polarization. The influence of the photon field polarization on the magnetic field dependence of the lead-system-lead and persistent current is illustrated in detail and connected with the properties of the many-body spectrum. It is further shown how the photon field influenced many-body spectrum affects the spatial charge arrangement and flow inside the ring. Concluding remarks will be presented in Sec. IV.

II. MODEL AND THEORY

In this section, we describe the central system potential V_S for the broad quantum ring and its connection to the leads. The electronic ring system is embedded in an electromagnetic cavity by coupling a many-level electron system with photons using the full photon energy spectrum of a single cavity mode. The central ring system is described by an MB system Hamiltonian $\hat{H}_S$ with a uniform perpendicular magnetic field in which the electron-electron interaction and the electron-photon coupling to the x- or y-polarized photon field is explicitly taken into account. We employ the TCL-GME approach to explore the nonequilibrium electronic transport when the system is coupled to leads by a transient switching potential.

A. Quantum ring connected to leads

The system under investigation is a broad quantum ring connected to left and right leads $l \in \{L, R\}$ with identical parabolic confining potentials

$$V_l(\mathbf{r}) = \tfrac{1}{2} m^* \Omega_0^2 y^2 \tag{1}$$

in which the characteristic energy of the confinement is $\hbar\Omega_0 = 1.0$ meV and $m^* = 0.067 m_e$ is the effective mass of an electron in GaAs-based material.

The quantum ring is embedded in the central system of length $L_x = 300$ nm situated between two contact areas that will be coupled to the external leads, as is depicted in Fig. 1. The system potential is described by

$$V_S(\mathbf{r}) = \sum_{i=1}^{6} V_i \exp\{-[\beta_{xi}(x - x_0)]^2 - (\beta_{yi} y)^2\} + \frac{1}{2} m^* \Omega_0^2 y^2, \tag{2}$$

with parameters from Table I.

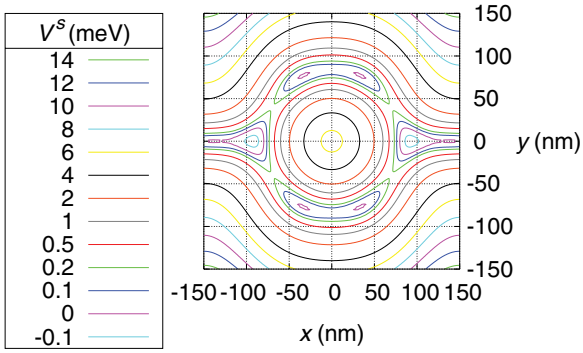

FIG. 1. (Color online) Equipotential lines in the central ring system connected to the left and right leads. Note that the isolines are refined close to the bottom of the ring structure.

B. Central system Hamiltonian

The time evolution of the closed system with respect to $t = 0$,

$$\hat{U}_S(t) = \exp\left(-\frac{i}{\hbar}\hat{H}_S t\right), \tag{3}$$

is governed by the MB system Hamiltonian[56]

$$\hat{H}_S = \int d^2r\ \hat{\psi}^\dagger(\mathbf{r})\left[\frac{1}{2m^*}\left\{\frac{\hbar}{i}\nabla + \frac{e}{c}[\mathbf{A}(\mathbf{r}) + \hat{\mathbf{A}}^{\rm ph}(\mathbf{r})]\right\}^2 + V_S(\mathbf{r})\right]\hat{\psi}(\mathbf{r}) + \hat{H}_{\rm ee} + \hbar\omega\hat{a}^\dagger\hat{a}\,. \tag{4}$$

The first term includes a constant magnetic field $\mathbf{B} = B\hat{\mathbf{z}}$, in Landau gauge being represented by $\mathbf{A}(\mathbf{r}) = -By\hat{\mathbf{x}}$. The second term is the exactly treated electron-electron interaction

$$\hat{H}_{\rm ee} = \int d^2r \int d^2r' \hat{\psi}^\dagger(\mathbf{r})\hat{\psi}^\dagger(\mathbf{r}')V_{\rm ee}(\mathbf{r},\mathbf{r}')\hat{\psi}(\mathbf{r}')\hat{\psi}(\mathbf{r})\,, \tag{5}$$

where

$$V_{\rm ee}(\mathbf{r},\mathbf{r}') = \frac{e^2}{2\kappa\sqrt{|\mathbf{r} - \mathbf{r}'|^2 + \eta^2}} \tag{6}$$

with $e > 0$ being the magnitude of the electron charge and $\eta = 1.0 \times 10^{-15}$ nm being a numerical regularization parameter. In addition, the last term in Eq. (4) indicates the quantized photon field, where $\hat{a}$ and $\hat{a}^\dagger$ are the photon annihilation and creation operators, respectively, and $\hbar\omega$ is the photon excitation energy. The photon field interacts with the electron system via the vector potential

$$\hat{\mathbf{A}}^{\rm ph}(\mathbf{r}) = A(\hat{a} + \hat{a}^\dagger)\begin{cases}\mathbf{e}_x, & \text{TE}_{011},\\ \mathbf{e}_y, & \text{TE}_{101},\end{cases} \tag{7}$$

TABLE I. Parameters of the central region ring potential.

i	V_i (meV)	β_{xi} (nm^{-1})	x_0 (nm)	β_{yi} (nm^{-1})
1	9.6	0.014	150	0
2	9.6	0.014	−150	0
3	11.1	0.0165	0	0.0165
4	−4.7	0.02	149	0.02
5	−4.7	0.02	−149	0.02
6	−4.924	0	0	0

for a longitudinally polarized (x-polarized) photon field (TE_{011}) or a transversely polarized (y-polarized) photon field (TE_{101}). The electron-photon coupling constant $g^{EM} = eAa_w\Omega_w/c$ scales with the amplitude A of the electromagnetic field. For reasons of comparison, we also consider results without photons in the system. In this case, $\hat{\mathbf{A}}^{ph}(\mathbf{r})$ and $\hbar\omega\hat{a}^\dagger\hat{a}$ drop out from the MB system Hamiltonian in Eq. (4).

C. Time-convolutionless generalized master equation approach

The TCL-GME[55] is an alternative non-Markovian master equation to the Nakajima-Zwanzig (NZ) equation,[57–60] which is *local* in time. We assume that the initial total statistical density matrix can be written as a product of the system and leads density matrices, before switching on the coupling to the leads,

$$\hat{W}(0) = \hat{\rho}_L \otimes \hat{\rho}_R \otimes \hat{\rho}_S(0), \tag{8}$$

with ρ_l, $l \in \{L,R\}$, being the normalized density matrices of the leads. The coupling Hamiltonian between the central system and the leads reads

$$\hat{H}_T(t) = \sum_{l=L,R} \int dq\ \chi^l(t)[\hat{\mathfrak{T}}^l(q)\hat{C}_{ql} + \hat{C}^\dagger_{ql}\hat{\mathfrak{T}}^{l\dagger}(q)]\,. \tag{9}$$

Here, $\hat{C}^\dagger_{ql}$ is the electron creation operator for state q and lead l and

$$\hat{\mathfrak{T}}^l(q) = \sum_{\alpha\beta} |\alpha)(\beta| \sum_a T^l_{qa}(\alpha|\hat{C}^\dagger_a|\beta) \tag{10}$$

with the creation operator $\hat{C}^\dagger_a$ for the single-electron state (SES) a in the central system, i.e., the eigenstate a of the first term of Eq. (4) with $\hat{\mathbf{A}}^{ph}(\mathbf{r}) = 0$. The coupling is switched on at $t = 0$ via the switching function

$$\chi^l(t) = 1 - \frac{2}{e^{\alpha^l t} + 1} \tag{11}$$

with switching parameter α^l. Equation (10) is written in the system Hamiltonian MB eigenbasis $\{|\alpha)\}$. The coupling tensor[56]

$$T^l_{qa} = \int_{\Omega^l_S} d^2r \int_{\Omega_l} d^2r'\ \psi^*_{ql}(\mathbf{r}')g^l_{aq}(\mathbf{r},\mathbf{r}')\psi^S_a(\mathbf{r}) \tag{12}$$

couples the extended lead SES $\{\psi_{ql}(\mathbf{r})\}$ with energy spectrum $\{\epsilon^l(q)\}$ to the system SES $\{\psi^S_a(\mathbf{r})\}$ with energy spectrum $\{E_a\}$ that reach into the contact regions,[59] Ω^l_S and Ω_l, of system and lead l, respectively, and

$$g^l_{aq}(\mathbf{r},\mathbf{r}') = g^l_0 \exp[-\delta^l_x(x-x')^2 - \delta^l_y(y-y')^2] \times \exp\left[-\frac{|E_a - \epsilon^l(q)|}{\Delta^l_E}\right]. \tag{13}$$

Here, g^l_0 is the lead coupling strength. In addition, δ^l_x and δ^l_y are the contact region parameters for lead l in x and y directions, respectively. Moreover, Δ^l_E denotes the affinity constant between the central system SES energy levels $\{E_a\}$ and the lead energy levels $\{\epsilon^l(q)\}$.

In this work, we derive the TCL-GME[55] in the Schrödinger picture. In this picture, the reduced density operator (RDO) of the system,

$$\hat{\rho}_S(t) = \mathrm{Tr}_L\mathrm{Tr}_R[\hat{W}(t)], \tag{14}$$

evolves to second order in the lead coupling strength in time via

$$\dot{\hat{\rho}}_S(t) = -\frac{i}{\hbar}[\hat{H}_S,\hat{\rho}_S(t)] - \left[\sum_{l=L,R}\int dq\ (\hat{\mathfrak{T}}^l(q),\hat{\Omega}^l(q,t)\hat{\rho}_S(t) - f[\epsilon^l(q)]\{\hat{\rho}_S(t),\hat{\Omega}^l(q,t)\}) + \mathrm{H.c.}\right] \tag{15}$$

with

$$\hat{\Omega}^l(q,t) = \frac{1}{\hbar^2}\chi^l(t)\exp\left[-\frac{i}{\hbar}t\epsilon^l(q)\right]\hat{U}_S(t)\hat{\Pi}^l(q,t)\hat{U}^\dagger_S(t), \tag{16}$$

$$\hat{\Pi}^l(q,t) = \int_0^t dt'\left\{\exp\left[\frac{i}{\hbar}t'\epsilon^l(q)\right]\chi^l(t')\hat{U}^\dagger_S(t')\hat{\mathfrak{T}}^{l\dagger}(q)\hat{U}_S(t')\right\}, \tag{17}$$

and $f(E)$ being the Fermi distribution function.

Comparing this equation to the corresponding NZ equation,[57–60]

$$\dot{\hat{\rho}}^{NZ}_S(t) = -\frac{i}{\hbar}\left[\hat{H}_S,\hat{\rho}^{NZ}_S(t)\right] - \left\{\sum_{l=L,R}\int dq\ [\hat{\mathfrak{T}}^l(q),\hat{\Omega}^l(q,t)] + \mathrm{H.c.}\right\} \tag{18}$$

with

$$\hat{\Omega}^l(q,t) = \frac{1}{\hbar^2}\chi^l(t)\hat{U}_S(t)\int_0^t dt'\left\{\exp\left[\frac{i}{\hbar}(t'-t)\epsilon^l(q)\right] \times \chi^l(t')\hat{\Pi}^l(q,t')\right\}\hat{U}^\dagger_S(t) \tag{19}$$

and

$$\hat{\Pi}^l(q,t') = \hat{U}^\dagger_S(t')\big(\hat{\mathfrak{T}}^{l\dagger}(q)\hat{\rho}^{NZ}_S(t') - f[\epsilon^l(q)]\big\{\hat{\rho}^{NZ}_S(t'),\hat{\mathfrak{T}}^{l\dagger}(q)\big\}\big)\hat{U}_S(t'), \tag{20}$$

we note that we reobtain the TCL equation, if we set

$$\hat{\rho}^{NZ}_S(t') = \hat{U}^\dagger_S(t-t')\hat{\rho}_S(t)\hat{U}_S(t-t'), \tag{21}$$

in Eq. (20) [which enters the kernel of Eq. (18)], but let $\hat{\rho}^{NZ}_S(t) = \hat{\rho}_S(t)$ in the first term of Eq. (18). In other words, in the Schrödinger picture, the NZ kernel takes the central system time propagated RDO (which lets it become convoluted), while the TCL kernel takes just the unpropagated RDO. The deviation between the two approaches is therefore only of relevance when the central system is far from a steady state and when the coupling to the leads is strong. It is our experience that the positivity conditions[61] for the MB state occupation probabilities in the RDO are satisfied to a higher system-lead coupling strength in the TCL case. The more involved quantum structure demands a stronger system-lead coupling than in our earlier work.[56] The numerical effort of the two approaches is of similar magnitude. Both cases allow for a t-independent inner time integral over t', which can be integrated successively

with increasing t (increasing integration domain).[62] The RDO is inside (NZ) or outside (TCL) of the inner time integral, but the required number of matrix multiplications is equal.

III. NONEQUILIBRIUM TRANSPORT PROPERTIES

In this section, we investigate the nonequilibrium electron transport properties through a quantum ring system, which is situated in a photon cavity and weakly coupled to leads. We assume GaAs-based material with electron effective mass $m^* = 0.067m_e$ and background relative dielectric constant $\kappa = 12.4$. We consider a single cavity mode with fixed photon excitation energy $\hbar\omega = 0.4$ meV. The electron-photon coupling constant in the central system is $g^{\mathrm{EM}} = 0.1$ meV. Before switching on the coupling, we assume the central system to be in the pure initial state with electron occupation number $N_{e,\mathrm{init}} = 0$ and photon occupation number $N_{\mathrm{ph,init}} = 1$ of the electromagnetic field.

An external perpendicular uniform magnetic field is applied through the central ring system and the lead reservoirs. The area of the central ring system is $A \approx 2 \times 10^4$ nm^2 so that the magnetic field corresponding to the flux quantum Φ_0 is $B_0 = \Phi_0/A \approx 0.2$ T. The temperature of the reservoirs is assumed to be $T = 0.5$ K. The chemical potentials in the leads are $\mu_L = 2$ meV and $\mu_R = 0.9$ meV leading to a source-drain bias window $\Delta\mu = 1.1$ meV. We let the affinity constant $\Delta_E^l = 0.25$ meV to be close to the characteristic electronic excitation energy in x direction. In addition, we let the contact region parameters for lead $l \in \{L,R\}$ in x and y directions be $\delta_x^l = \delta_y^l = 4.39 \times 10^{-4}$ nm^{-2}. The system-lead coupling strength $g_0^l = 0.2058$ meV nm$^{-3/2}$.

There are several relevant length and time scales that should be mentioned. The two-dimensional magnetic length is $l = [c\hbar/(eB)]^{1/2} = 25.67[B(\mathrm{T})]^{-1/2}$ nm. The ring system is parabolically confined in the y direction with characteristic energy $\hbar\Omega_0 = 1.0$ meV leading to a modified magnetic length scale

$$a_w = \left(\frac{\hbar}{m^*\Omega_0}\right)^{1/2} \frac{1}{\sqrt[4]{1+[eB/(m^*c\Omega_0)]^2}} = \frac{33.74}{\sqrt[4]{1+2.982[B(\mathrm{T})]^2}}\ \mathrm{nm}. \tag{22}$$

Correspondingly, the system-lead coupling strength is then $g_0^l a_w^{3/2} = 39.85$ meV for magnetic field $B = 0.1$ T and $g_0^l a_w^{3/2} = 38.22$ meV for magnetic field $B = 0.225$ T. The time scale for the switching on of the system-lead coupling is $(\alpha^l)^{-1} = 3.291$ ps, the single-electron state (1ES) charging time scale $\tau_{1\mathrm{ES}} \approx 30$ ps, and the two-electron state (2ES) charging time scale $\tau_{2\mathrm{ES}} \gg 200$ ps described in the sequential tunneling regime. We study the transport properties for $0 \leqslant t < \tau_{2\mathrm{ES}}$, when the system has not yet reached a steady state.

In order to understand the nonequilibrium dynamical behavior of the charge distribution in the system, we define the time-dependent magnitude of charge on the left part ($x < 0$) of the ring,

$$Q_S^L(t) = \int_{-\frac{L_x}{2}}^{0} dx \int_{-\infty}^{\infty} dy\ \rho(\mathbf{r},t), \tag{23}$$

and the time-dependent magnitude of charge on the right part ($x > 0$) of the ring

$$Q_S^R(t) = \int_{0}^{\frac{L_x}{2}} dx \int_{-\infty}^{\infty} dy\ \rho(\mathbf{r},t)\,. \tag{24}$$

The space- and time-dependent charge density,

$$\rho(\mathbf{r},t) = \mathrm{Tr}[\hat{\rho}_S(t)\hat{\rho}(\mathbf{r})], \tag{25}$$

is the expectation value of the charge density operator

$$\hat{\rho}(\mathbf{r}) = e\hat{\psi}^\dagger(\mathbf{r})\hat{\psi}(\mathbf{r}). \tag{26}$$

In order to explore the magnetic field influence on the charge currents from and into the leads, we define the charge current from the left lead into the system by

$$I_L(t) = \mathrm{Tr}\big[\dot{\hat{\rho}}_S^L(t)\hat{Q}\big]\,. \tag{27}$$

Here, $\hat{Q} = e\hat{N}$ is the charge operator with number operator $\hat{N}$ and the time derivative of the RDO in the MB basis due to the coupling to the lead $l \in \{L,R\}$:

$$\dot{\rho}_S^l(t) = \int dq\ [\mathfrak{T}^l(q),(\Omega^l(q,t)\rho_S(t) - f[\epsilon^l(q)]\{\rho_S(t),\Omega^l(q,t)\})] + \mathrm{H.c.}. \tag{28}$$

Similarly, the charge current from the system into the right lead can be expressed as

$$I_R(t) = -\mathrm{Tr}\big[\dot{\hat{\rho}}_S^R(t)\hat{N}\big]. \tag{29}$$

To get more insight into the local current flow in the ring system, we define the top local charge current through the upper arm ($y > 0$) of the ring

$$I_{\mathrm{top}}(t) = \int_0^\infty dy\ j_x(x=0,y,t) \tag{30}$$

and the bottom local charge current through the lower arm ($y < 0$) of the ring

$$I_{\mathrm{bottom}}(t) = \int_{-\infty}^0 dy\ j_x(x=0,y,t)\,. \tag{31}$$

Here, the charge current density,

$$\mathbf{j}(\mathbf{r},t) = \begin{pmatrix} j_x(\mathbf{r},t) \\ j_y(\mathbf{r},t) \end{pmatrix} = \mathrm{Tr}[\hat{\rho}_S(t)\hat{\mathbf{j}}(\mathbf{r})], \tag{32}$$

is given by the expectation value of the charge current density operator,

$$\hat{\mathbf{j}}(\mathbf{r}) = \hat{\mathbf{j}}_p(\mathbf{r}) + \hat{\mathbf{j}}_d(\mathbf{r}), \tag{33}$$

decomposed into the paramagnetic charge current density operator,

$$\hat{\mathbf{j}}_p(\mathbf{r}) = \frac{e\hbar}{2mi}\{\hat{\psi}^\dagger(\mathbf{r})[\nabla\hat{\psi}(\mathbf{r})] - [\nabla\hat{\psi}^\dagger(\mathbf{r})]\hat{\psi}(\mathbf{r})\}, \tag{34}$$

and the diamagnetic charge current density operator,

$$\hat{\mathbf{j}}_d(\mathbf{r}) = \hat{\mathbf{j}}_d^{\mathrm{mag}}(\mathbf{r}) + \hat{\mathbf{j}}_d^{\mathrm{ph}}(\mathbf{r}). \tag{35}$$

The latter consists of a magnetic component,

$$\hat{\mathbf{j}}_d^{\mathrm{mag}}(\mathbf{r}) = \frac{e^2}{m}\mathbf{A}(\mathbf{r})\hat{\psi}^\dagger(\mathbf{r})\hat{\psi}(\mathbf{r}), \tag{36}$$

and photonic component,

$$\hat{\mathbf{j}}_d^{\rm ph}(\mathbf{r}) = \frac{e^2}{m}\hat{\mathbf{A}}^{\rm ph}(\mathbf{r})\hat{\psi}^\dagger(\mathbf{r})\hat{\psi}(\mathbf{r}). \tag{37}$$

Furthermore, to understand better the driving schemes of the dynamical transport features, we define the total local charge current

$$I_{\rm tl}(t) = I_{\rm top}(t) + I_{\rm bottom}(t) \tag{38}$$

and circular local charge current

$$I_{\rm cl}(t) = \tfrac{1}{2}[I_{\rm top}(t) - I_{\rm bottom}(t)]. \tag{39}$$

Below, we shall explore the influence of the applied magnetic field and the photon field polarization on the nonequilibrium quantum transport in terms of the above time-dependent charges and currents in the broad quantum ring system connected to leads.

A. Photons with x polarization

In this section, we focus on our results for x-polarized photon field. Figure 2 shows the MB energy spectrum of the system Hamiltonian $\hat{H}_S$ including the electron-electron and electron-photon interactions. The MB-energy levels are assigned different colors according to their electron content N_e. The bias window (solid black lines) contains $(\mu_L - \mu_R)/(\hbar\omega)$ zero-electron states (green dots) and several SESs (red dots). However, even in the sequential tunneling regime, SESs outside the bias window can contribute to the transport due to the photon perturbation and the time dependency of the coupling to the leads. In order to estimate the energetic

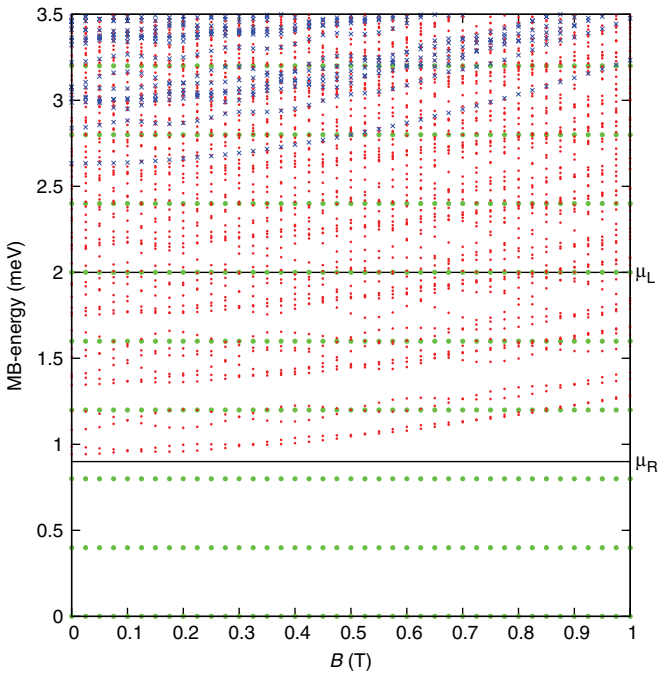

FIG. 2. (Color online) MB energy spectrum of system Hamiltonian $\hat{H}_S$ vs magnetic field B in units of tesla (T). The states are differentiated according to their electron content N_e: zero-electron states ($N_e = 0$, 0ES, green dots), single-electron states ($N_e = 1$, 1ES, red dots) and two-electron states ($N_e = 2$, 2ES, blue crosses). The photon field is x polarized.

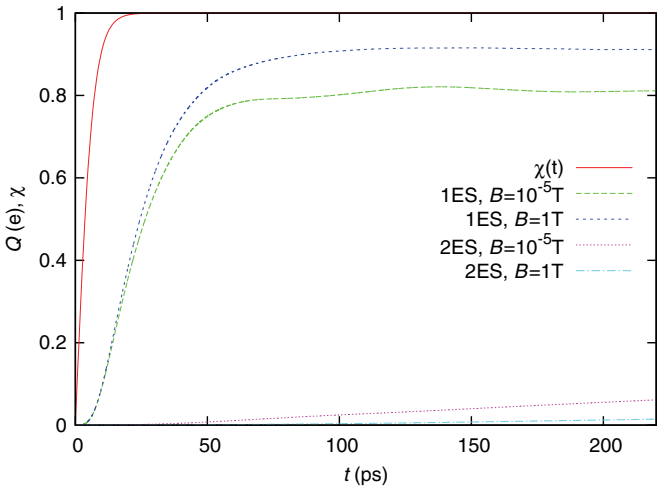

FIG. 3. (Color online) Switching function $\chi^l(t)$ (solid red), charge of all 1ES for $B = 10^{-5}$ T (long-dashed green) and $B = 1.0$ T (short-dashed blue), and charge of all 2ES for $B = 10^{-5}$ T (dotted purple) and $B = 1.0$ T (dash-dotted cyan) as a function of time. The photon field is x-polarized.

capability of the two electron states (2ES, blue crosses) to contribute to the transport, their energy difference to the SES has to be considered. This energy difference can fall into the bias window.

Our specific ring geometry has two main effects on the spectrum. First, the rotation symmetry violation due to the contact regions leads to avoided crossings at integer flux quanta leaving only the half-integer flux quanta crossings. For the latter, wave functions of odd and even quantum numbers of magnetic moment[18] cross, which therefore have opposite and equal phases at the contact regions, respectively, thus leaving them uninfluenced by the rotation symmetry violation. It can be seen from an analysis of the wave functions with magnetic flux that the magnetic moment remains unchanged and clearly defined for the crossings at half-integer flux quantum, while a gradual change in the magnetic moment quantum number by an even number is observable at the avoided crossings. Second, the finite ring width allows for small state-dependent variations of the crossing period B_0.

Figure 3 illustrates the central region charging of 1ES and 2ES as a function of time. It demonstrates the earlier mentioned time scales $(\alpha^l)^{-1} = 3.291$ ps, $\tau_{\rm 1ES} \approx 30$ ps and $\tau_{\rm 2ES} \gg 200$ ps. The 2ES are occupied slower than the 1ES indicating the sequential tunneling processes and the 2ES energetic shift by the Coulomb interaction. The effect is more pronounced for higher magnetic field due to the larger energy difference of the 2ES with respect to the 1ES (see Fig. 2). The total charging has slowed down by more than one order of magnitude around $t = 200$ ps.

In Fig. 4, we show the current from the left lead into the ring system I_L (solid red curve) and the current from the ring system to the right lead I_R (long-dashed green curve) as a function of magnetic field at time $t = 200$ ps. The similar values of $I_L(B)$ and $I_R(B)$ indicate the slow down in the total charging. We see clear oscillations of the current with period $B_0 \approx 0.2$ T: the first minimum current at $B = 0.1$ T corresponds to the situation of a half-flux quantum, while the maximum current

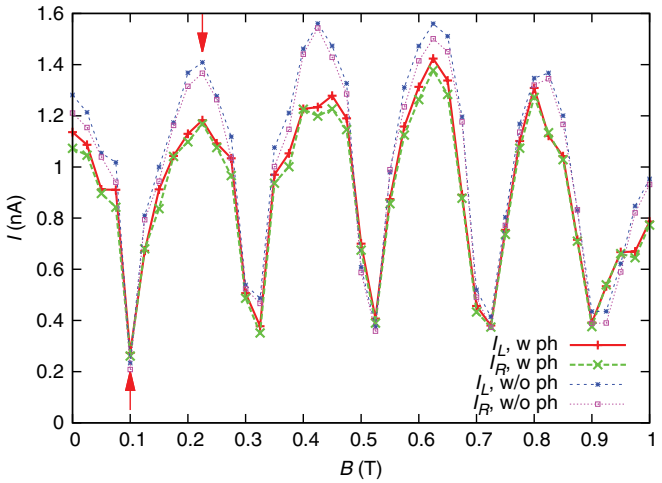

FIG. 4. (Color online) The left charge current I_L (solid red) and the right charge current I_R (long-dashed green) vs the magnetic field with (w) x-polarized photon field at $t = 200$ ps. For comparison: left charge current I_L (short-dashed blue) and right charge current I_R (dotted purple) in a purely electronic central system, i.e., without (w/o) photon cavity.

at $B = 0.225$ T is corresponding to the case of one flux quantum. Although the oscillations could be classified as being of Aharonov-Bohm (AB) type,[12–14] modifications by the electron-electron correlation effects and the nonequilibrium situation may not be neglected. In addition, the electron-photon coupling suppresses the constructive interference of AB phases in the integer flux quantum situation as can be seen from a comparison with the purely electronic system results in Fig. 4 (short-dashed blue and dotted purple curve).

In Fig. 5, we illustrate the normalized charge current density vector field $\mathbf{j}(\mathbf{r},t)$ in the central quantum ring system in the long-time response regime $t = 200$ ps, i.e., when the 2ES get charged. For magnetic field $B = 0.1$ T, a clear counterclockwise vortex located close to the left lead can be found dominating the current flow pattern in the central ring system as shown in Fig. 5(a).[16] The vortex circulation direction is determined by the Lorentz force, while the vortex area is too small to see effects of the threaded magnetic flux. It is important to realize that the vortex circulation direction in combination with the geometrical position of the vortex and the current continuity condition, favors clockwise current direction for the ring system. For magnetic field $B = 0.225$ T, the counterclockwise vortex appears relatively weak being present at both left and right lead connection areas as shown in Fig. 5(b), while the total local current through the whole central system from the left to the right lead is large. Additionally, for a later comparison with the y-polarized photon field, Fig. 5(c) shows the current density for $B = 0.425$ T (two flux quanta), which is similar to Fig. 5(b) (one flux quanta).

Figure 6 illustrates the time-dependent charge on the left part of the ring $Q_S^L(t)$ and the time-dependent charge on the right part of the ring $Q_S^R(t)$. In the half-integer flux quantum case $B = 0.1$ T shown in Fig. 6(a), both Q_S^L and Q_S^R are increasing almost monotonically in time. In the long-time response regime $t = 200$ ps, $Q_S^L(t) = 0.742e$ is much higher than $Q_S^R(t) = 0.234e$.

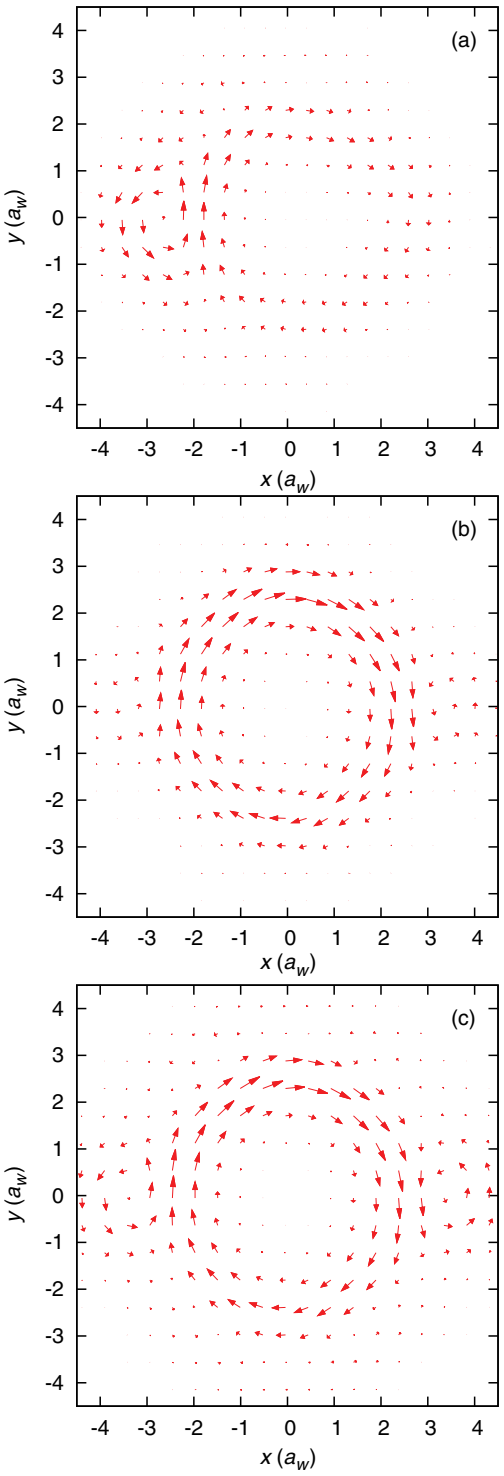

FIG. 5. (Color online) Normalized charge current density vector field in the central system for (a) $B = 0.1$ T, (b) $B = 0.225$ T, and (c) $B = 0.425$ T at $t = 200$ ps in the case of x-polarized photon field.

In the integer flux quantum case $B = 0.225$ T shown in Fig. 6(b), we find oscillating behavior of the charge between the left and right parts of the quantum ring. The oscillation amplitude is decreasing in time due to the dissipation effects caused by the coupling to the leads. In the long-time response regime $t = 200$ ps, $Q_S^L(t) = 0.423e$ is of similar magnitude as $Q_S^R(t) = 0.446e$ differently from the half-integer flux quantum

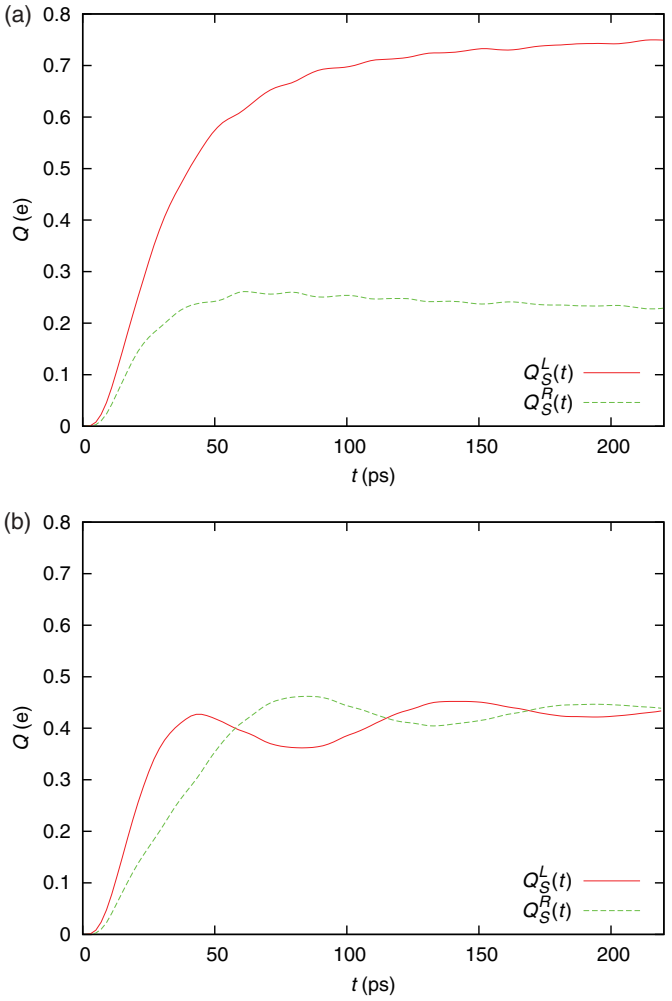

FIG. 6. (Color online) Charge in the left $[Q_S^L(t)]$ or right $[Q_S^R(t)]$ half of the central quantum ring system as a function of time for (a) $B = 0.1$ and (b) 0.225 T. The photon field is x-polarized.

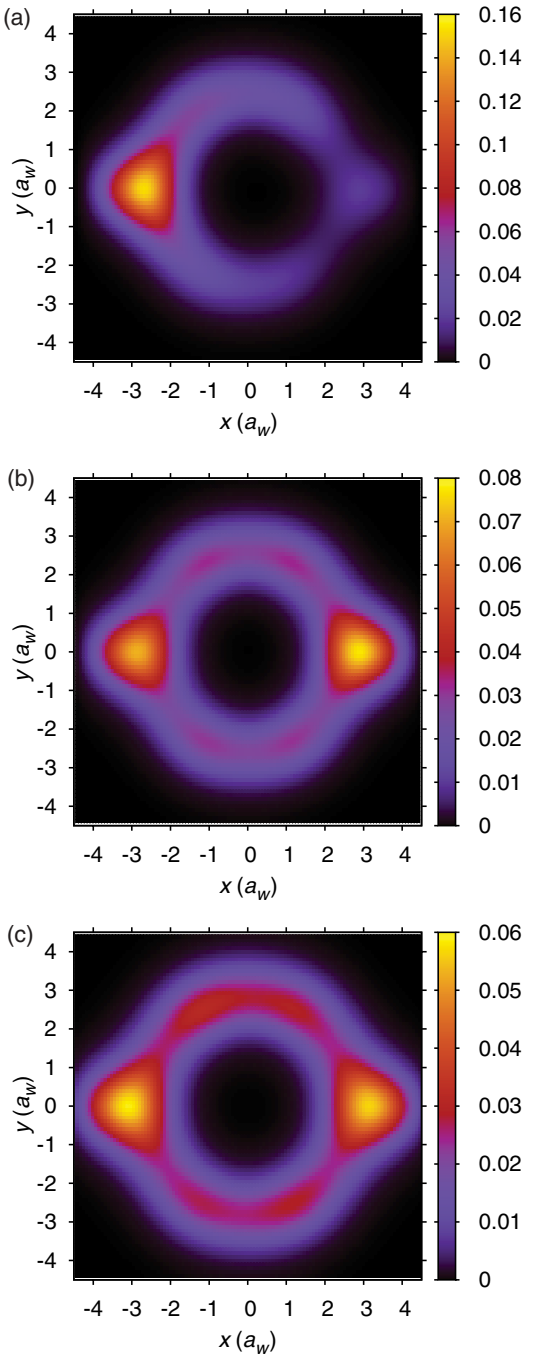

FIG. 7. (Color online) Charge density distribution $\rho(\mathbf{r},t)$ (e/a_w^2) in the central system for (a) $B = 0.1$, (b) 0.225, and (c) 0.425 T in the x-polarized photon field case at $t = 200$ ps.

case. The characteristic energy $\delta E_Q \approx 0.04$ meV of the charge oscillating period $\tau \approx 100$ ps agrees well with the MB energy difference of the mostly occupied MB states. As we find these MB states not only to correspond to the elements of the RDO causing this oscillation, but also to influence the current magnitude both due to AB and photon effects, we consider these states to be of particular interest. The MB energy levels are $E_{10}^x = 1.4038$ meV and $E_9^x = 1.3664$ meV such that $\Delta E_{9,10}^x = 0.0374$ meV. The corresponding two-level (TL) oscillation period of the closed system would be $\tau_{\rm TL}^0 = 111$ ps. In the nonequilibrium open system, the TL oscillation period is $\tau_{\rm TL}^L = 94$ ps or $\tau_{\rm TL}^R = 100$ ps when we take the time intervals between the first and second maxima of $Q_S^L(t)$ and $Q_S^R(t)$, respectively. The full numerical calculation including all MB levels shown in Fig. 6(b) yields the left and right charge oscillation periods, $\tau^L = 96$ ps and $\tau^R = 110$ ps, respectively. The system is far from equilibrium at the earlier maximum, thus reducing, in particular, the left period $\tau_{\rm TL}^L$ with respect to $\tau_{\rm TL}^0$. Furthermore, we find that also the other MB states change the periods when comparing τ^L with $\tau_{\rm TL}^L$ and τ^R with $\tau_{\rm TL}^R$.

Figure 7 shows the charge density distribution in the central quantum ring system with the magnetic field (a) $B = 0.1$, (b) 0.225, and (c) 0.425 T at $t = 200$ ps. In the case of $B = 0.1$ T (half-flux quantum) shown in Fig. 6(a), the electrons are highly accumulated on the left-hand side of the quantum ring with very weak coupling to the right lead, and hence strongly blocking the left charge current and suppressing the right charge current, as it was shown previously in Fig. 4 (marked by the up arrow). The electron dwell time on the left-hand side of the ring is enhanced relative to the electron dwell time on the right-hand side of the ring due to destructive

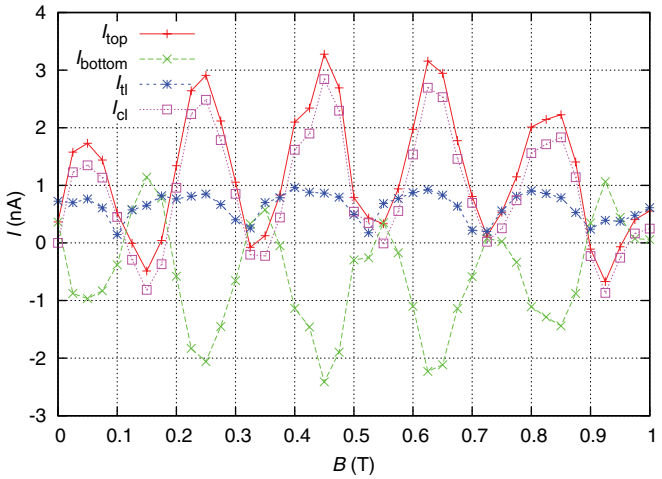

FIG. 8. (Color online) Local current through the top arm of the ring I_{top} (solid red), local current through the bottom arm of the ring I_{bottom} (long-dashed green), total local current I_{tl} (short-dashed blue), and the circular local current I_{cl} (dotted purple) versus the magnetic field averaged over the time interval [180,220] ps in the case of x-polarized photon field.

phase interference on the right-hand side suppressing also the evoked vortex there [see Fig. 5(a)].

In the $B = 0.225$ T case (one flux quantum) shown in Fig. 7(b), the electrons are nearly equally well accumulated on both sides of the quantum ring. This phenomenon is related to the manifestation of current peaks observed in Fig. 4 (marked by the down arrow) as the constructive phase interference enhances the likelihood for electrons to flow through the quantum ring to the right-hand side of the central system and further to the right lead. Additionally, for a later comparison, Fig. 7(c) shows the charge density for $B = 0.425$ T (two flux quanta), which is similar to Fig. 7(b) (one flux quantum).

In Fig. 8, we show the magnetic field dependence of the partial local currents I_{top} and I_{bottom} through the top and bottom arms, the total local current I_{tl} across $x = 0$, and the circular local current I_{cl}, which are convenient tools to study the relative importance of local "persistent" current flows induced by the magnetic field in the long-time response transient time regime. We would like to bring attention to the fact that charge balances like $\dot{Q}_L = I_L - I_{tl}$ and $\dot{Q}_R = I_{tl} - I_R$ would not be satisfied for the local current I_{tl}. This is because the SES that are filled from the left lead or emptied to the right lead are in general not restricted to a single half of the central system, but extended over the whole system. The total local current (short-dashed blue) through the two current arms, I_{tl}, is strongly suppressed in the case of half-integer flux quanta showing a very similar behavior to the nonlocal currents I_L and I_R (see Fig. 4). This is because the destructive interference in the quantum ring enhances the back scattering for magnetic flux with half-integer quanta.

The "persistent" circular local current (dotted purple) is usually larger in magnitude than the total local current leading to a different top and bottom local flow direction. In the absence of magnetic field $B = 0$, the circular current, however, is identical to zero due to the symmetric situation for both ring arms. It is interesting to note that the circular local current I_{cl} reaches 1.347 nA for less than half a flux quantum (at $B = 0.05$ T), increases further until $B = 0.45$ T with a maximum value $\max|I_{cl}| = 2.844$ nA and decreases again for $B > 0.45$ T. The magnetic component of the diamagnetic part of the circular local current increases linearly with the magnetic field B, but the paramagnetic part guarantees a behavior, which is closer to being periodic with the flux quantum. The periodic structure appears also for a ring of infinitesimal width,[17] but is shifted here toward clockwise circulation due to the vortices in Fig. 5. In the case of high magnetic field regime ($B > 0.45$ T), a comparison with Fig. 2 shows that the different flux periods of different MB-states in the finite-width ring lead to destructive interference effects reducing the periodic oscillations considerably.

B. Photons with y polarization

In this section, we focus on the y-polarized photon field situation and compare with the results for the x-polarized photon field. Figure 9 shows the MB energy spectra of the system Hamiltonian $\hat{H}_S$ in the case of (a) x-polarized and (b) y-polarized photon field. We note in passing that Fig. 9(a) magnifies a part of the MB spectrum of Fig. 2. The mostly occupied levels are the two levels around 1.4 meV. In the cases of both x- and y-polarized photon field, we see the MB energy degeneracy around $B = 0.1$ and 0.325 T related to the destructive AB phase interference. However, in the case of y polarization, an extra MB energy degeneracy is found at $B = 0.425$ T. This degeneracy is related to a current dip coming from *photonic* suppression, i.e., it is not related to AB oscillations.

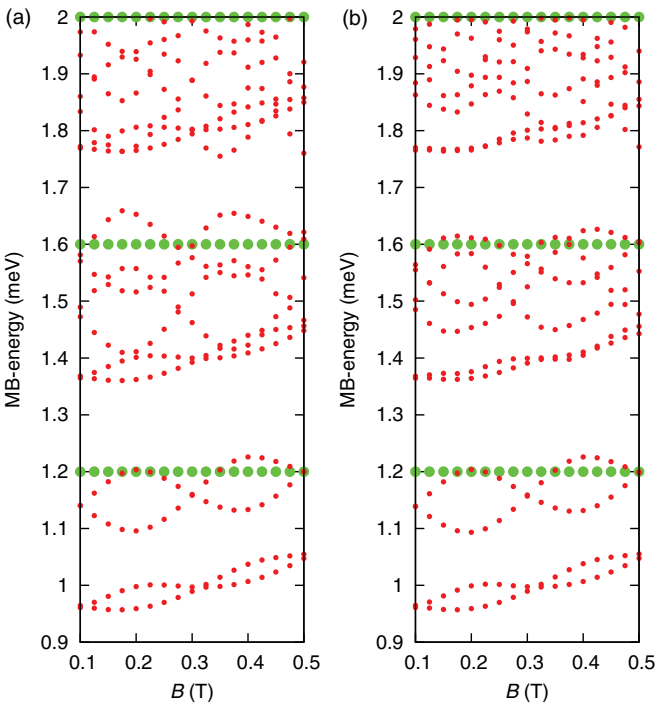

FIG. 9. (Color online) MB energy spectrum of the system Hamiltonian $\hat{H}_S$ vs magnetic field B within the bias window energy range for (a) x-polarized and (b) y-polarized photon field. The states are differentiated according to their electron content N_e: zero-electron ($N_e = 0$, 0ES, green dots) and single-electron ($N_e = 1$, 1ES, red dots) states.

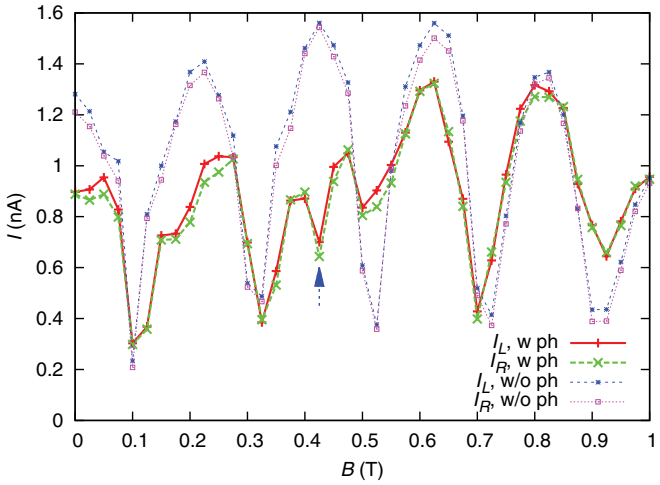

FIG. 10. (Color online) Left charge current I_L (solid red) and right charge current I_R (long-dashed green) vs the magnetic field with (w) y-polarized photon field at $t = 200$ ps. For comparison: left charge current I_L (short-dashed blue) and right charge current I_R (dotted purple) in a purely electronic central system, i.e., without (w/o) photon cavity.

Figure 10 shows the left charge current I_L (solid red) and the right charge current I_R (long-dashed green) as a function of magnetic field at $t = 200$ ps. It is eye catching that the oscillation amplitude and extrema positions show more unexpected features than in the case of x-polarized photon field. In particular, we would like to point out that the magnetic field dependence of the charge current exhibits a pronounced dip at $B = 0.425$ T (two flux quanta) in the case of a y-polarized photon field that is not present in the case of an x-polarized photon field. The dip structure is due to the above mentioned extra degeneracy of the MB energy spectrum, which strongly suppresses the photon-assisted tunneling properties. Furthermore, the charge current can be enhanced by the y-polarized photon field at magnetic field with half-integer flux quantum.

Figure 11 shows the normalized charge current density vector field $\mathbf{j}(\mathbf{r},t)$ in the central ring system for the magnetic field, (a) $B = 0.1$, (b) 0.225, and (c) 0.425 T, in the long-time response regime $t = 200$ ps. For magnetic field $B = 0.1$ T, a clear counterclockwise vortex can be found being associated with a long-living localized state, which is strongly dominating the current flow pattern in the central ring system, as is shown in Fig. 11(a). However, for magnetic field $B = 0.225$ T, this counterclockwise vortex appears weaker relative to the total local current, but is present at both contact regions as shown in Fig. 11(b). Figures 11(a) and 11(b) are similar to Figs. 5(a) and 5(b) meaning that the local current flow is mainly governed by AB interference with the photon polarization having only a minor effect.

Figure 11(c) shows the current density field for $B = 0.425$ T (two flux quanta), which is similar to the half-integer flux quanta case Fig. 11(a) and not to the integer flux quanta case Fig. 11(b). This similarity is only found for y polarization. [Instead for x polarization, the integer flux quanta cases Figs. 5(a) and 5(b) are found to be similar.] The charge flow at $B = 0.425$ T for y polarization is therefore not predicted by the AB effect, but is caused by the influence of the y-polarized

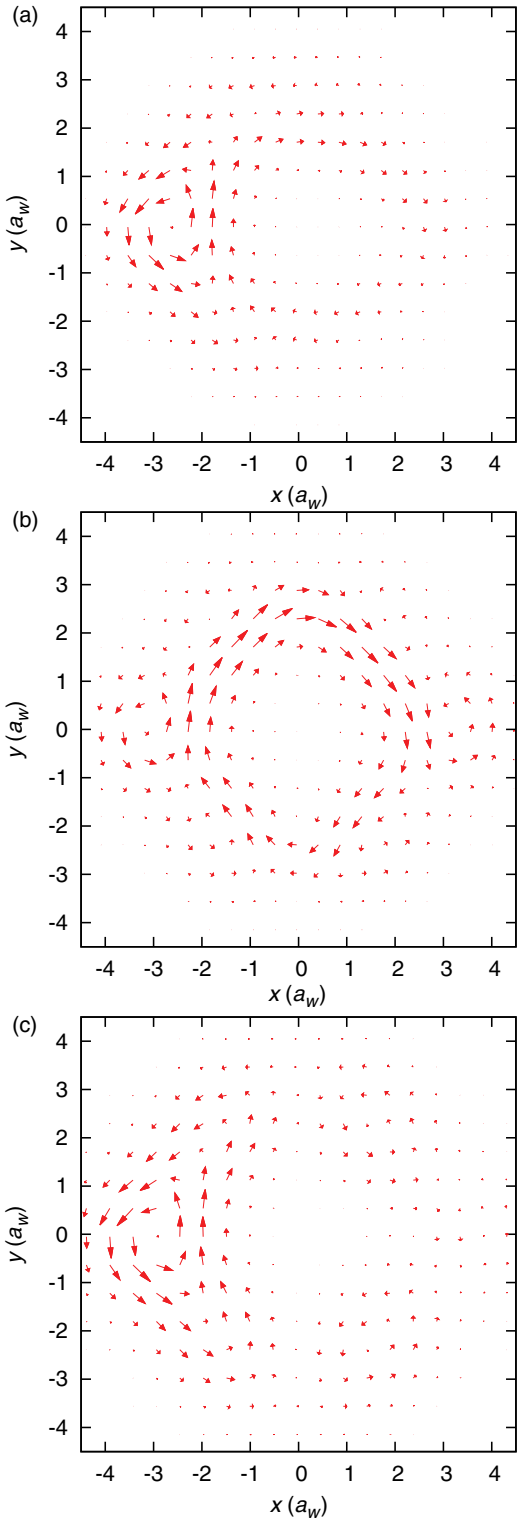

FIG. 11. (Color online) Normalized charge current density vector field in the central system for (a) $B = 0.1$, (b) 0.225, and (c) 0.425 T at $t = 200$ ps in the case of y-polarized photon field.

photons. However, any MB spectrum degeneracy of the mostly occupied MB states [see Fig. 9(b)], whether it originates from the AB effect [see Fig. 11(a)] or the photons [see Fig. 11(c)], influences the local current flow structure in a similar way.

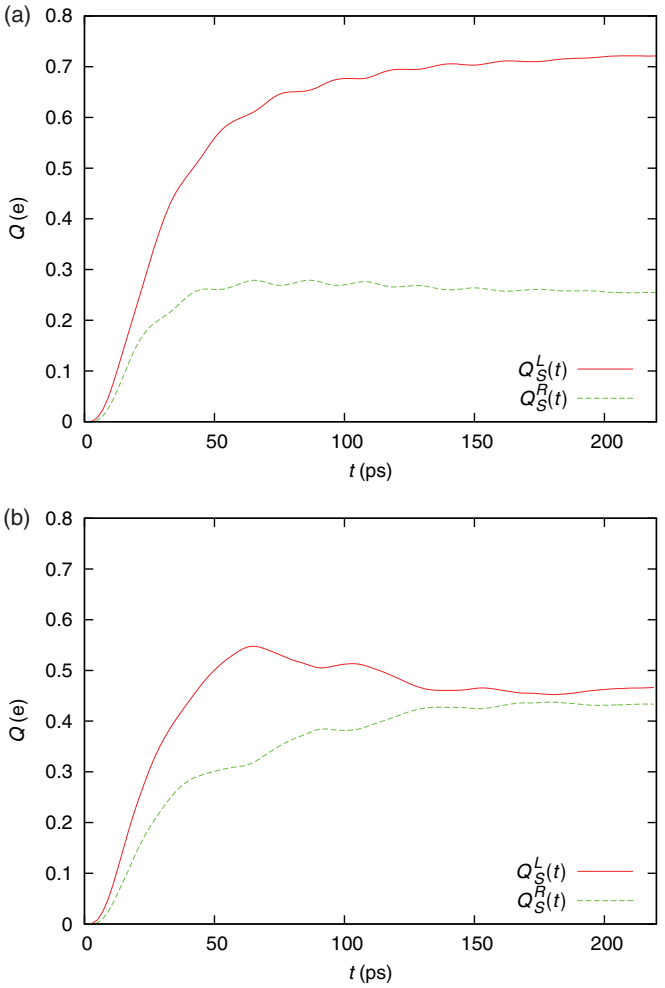

FIG. 12. (Color online) Charge in the left $[Q_S^L(t)]$ or right $[Q_S^R(t)]$ half of the central system as a function of time for (a) $B = 0.1$ T and (b) $B = 0.225$ T. The photon field is y polarized.

Figure 12 shows the time evolution of $Q_S^L(t)$ and $Q_S^R(t)$. In the long-time response regime at time $t = 200$ ps, the picture is very similar to the x-polarized photon field case: for $B = 0.1$ T, the charge is mainly accumulated at the left-hand side, $Q_S^L = 0.720e$ and $Q_S^R = 0.256e$ and for $B = 0.225$ T, the left and right charges are of similar magnitude, $Q_S^L = 0.462e$ and $Q_S^R = 0.431e$. However, in the $B = 0.225$ T case, the MB energies of the mostly occupied MB levels are $E_{10}^y = 1.3846$ meV and $E_9^y = 1.3683$ meV such that $\Delta E_{9,10}^y = 0.0163$ meV. Thus the energy level difference of the mostly occupied MB levels is only 44% of the case of x-polarized photon field: $E_{9,10}^y \approx 0.44 \times E_{9,10}^x$. The corresponding TL oscillation period of the closed system would be $\tau_{\mathrm{TL}}^0 = 254$ ps. The oscillation period is too long to be observed clearly in Fig. 12(b), but we know from the analysis of the TL system defined by the two mostly occupied states that the low-frequency oscillation starts with its first maximum of $Q_S^L(t)$ at $t = 65$ ps. Our findings suggest that the energy difference of the two mostly occupied levels controls not only the charge distribution, but also photonic suppressions of the AB current. The different connectivity (probability density on the left or right ring part) to the leads found within the TL dynamic suggests that the probability of a photon coupled electron transition between these levels plays a major role in understanding the photonic modifications of the AB current pattern.

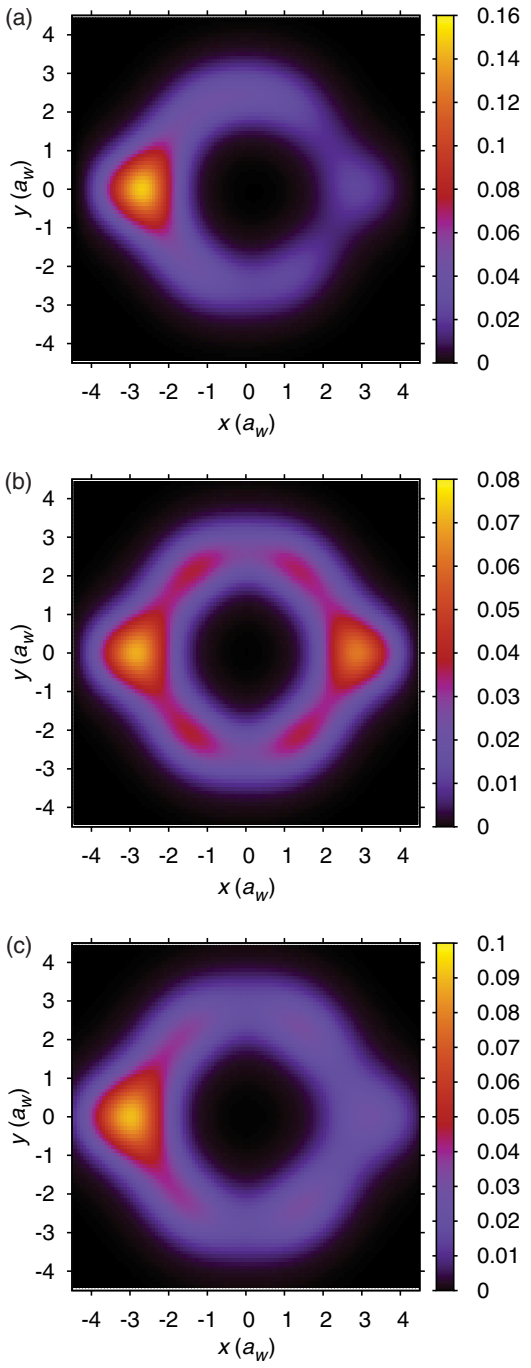

FIG. 13. (Color online) Charge density distribution $\rho(\mathbf{r},t)$ (e/a_w^2) in the central system for (a) $B = 0.1$, (b) 0.225, and (c) 0.425 T in the y-polarized photon field case at $t = 200$ ps.

Figure 13 shows the charge density distribution in the central ring system for magnetic field (a) $B = 0.1$, (b) 0.225, and (c) 0.425 T at $t = 200$ ps. In the case of $B = 0.1$ T shown in Fig. 13(a), the electrons are highly accumulated on the left-hand side of the quantum ring with very weak coupling to the right lead, and hence strongly blocking the left charge current and suppressing the right charge current.

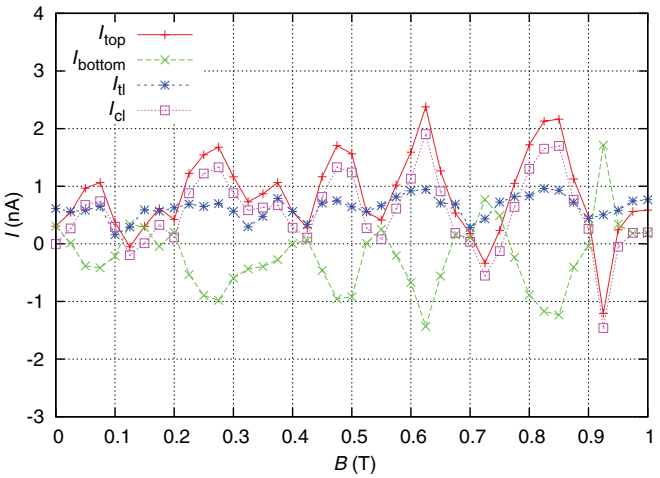

FIG. 14. (Color online) Local current through the top I_{top} (solid red) and bottom I_{bottom} (long-dashed green) ring arms and total I_{tl} (short-dashed blue) and circular I_{cl} (dotted purple) local currents vs the magnetic field and averaged over the time interval [180,220] ps in the case of y-polarized photon field.

In the integer flux quanta case of $B = 0.225$ T shown in Fig. 13(b), the electrons are equally well accumulated on both sides of the quantum ring. This situation is related to the manifestation of the current peaks observed in Fig. 10 by enhancement of the likelihood for electrons to flow through the quantum ring to the right-hand side of the central system and further to the right lead.

Figure 13(c) shows the charge density for $B = 0.425$ T (two flux quanta), which is similar to the half-integer flux quanta case Fig. 13(a). This feature is therefore not predicted by the AB effect, but is caused by the influence of the y-polarized photons. However, any MB spectrum degeneracy of the mostly occupied MB states [see Fig. 9(b)], whether it originates from the AB effect [see Fig. 13(a)] or the photons [see Fig. 13(c)], influences the density distribution in a similar way.

In Fig. 14, we show the magnetic field dependence of the local currents I_{top} and I_{bottom} through the top and bottom arms, respectively, the total local current I_{tl} across $x = 0$, and the circular local current I_{cl}. The local current through the two current arms, I_{tl}, is suppressed in the case of half-integer flux quanta showing a similar behavior to the nonlocal currents I_L and I_R (see Fig. 10). We find more irregularities due to the stronger effective influence of the y-polarized photon field than for x polarization. It is interesting to note that the current suppression dip at $B = 0.425$ T (marked by the blue arrow in Fig. 10) appears also in the local current (blue short-dashed curve) flowing through both ring arms from the left to the right.

The "persistent" circular local current reaches a maximum absolute value of max $|I_{cl}| = 1.905$ nA at $B = 0.625$ T, which is by 0.939 nA smaller than for x polarization. It is clearly visible from a comparison of Figs. 14 and 8 that the circular current is considerably smaller than in the x-polarized photon case, while the total local current is of the same order. Thus the capability of the magnetic field to drive a rotational ring current is weakened by having the electromagnetic field y-polarized. In particular, this can be said about the diamagnetic part of the circular local current leading to the much smaller value $I_{cl} = 0.675$ nA at low magnetic field $B = 0.05$ T. The periodicity of the circular local current is preserved better for x-polarized photon field as is for the total local current emphasizing the perturbing influence of the y-polarized photon field.

IV. CONCLUDING REMARKS

We have presented a time-convolutionless generalized master equation formalism that allows us to calculate the nonequilibrium transport of Coulomb interacting electrons through a broad quantum ring in a photon cavity under the influence of a uniform perpendicular magnetic field. The topologically nontrivial broad ring geometry allows for substantial electron-electron correlations relative to their kinetic energy and, hence, a large basis is required for sufficient numerical accuracy. The central quantum ring 1ES are charged quickly. Electron-electron correlation and sequential tunneling slow down the 2ES charging in the long-time response regime. Aharonov-Bohm charge current oscillations can be recognized in the long-time response regime with magnetic field period $B_0 = \Phi_0/A$, which is related to the flux quantum Φ_0 and ring area A.

In the case of x-polarized photon field, we have found charge oscillations between the left and right parts of the quantum ring when the magnetic field is associated with integer flux quanta. The oscillation frequency agrees well with the energy difference of the two mostly occupied states. The relatively high energy difference for x-polarized photons is related to a relatively high transient current through the ring. The amplitude of the charge oscillations through the quantum ring is decreasing in time due to dissipation effects caused by the coupling to the leads. Usually, the local current through the upper ring arm exhibits opposite sign to the local current through the lower ring arm. Hence the "persistent" circular local current is usually larger than the total local charge current through both ring arms from the left to the right. The persistent current shows a periodic behavior with magnetic field, but with a tendency to clockwise rotation due to the contact region vortex structure.

In the case of y-polarized photon field, the magnetic field dependence of the left and right charge current exhibits a pronounced dip at magnetic field $B = 0.425$ T corresponding to two flux quanta that is therefore clearly not related to the Aharonov-Bohm effect. The dip is associated with a degeneracy of the two mostly occupied MB states at magnetic field associated with two flux quanta. The additional level crossing appears only for y-polarized photons, but influences the spatial distribution of the charge density and flow similarly to any other MB degeneracy. The generally lower energy difference of the two mostly occupied MB states in the case of y polarization perturbs the constructive phase interference condition for the bias driven charge flow through the quantum device and decreases the persistent current magnitude.

In conclusion, we have demonstrated for our ring geometry that y-polarized photons perturb our system stronger than x-polarized photons, suppressing or enhancing magnetic field induced and bias-driven currents and perturbing flux periodicity beyond finite width effects. It is interesting to compare these findings to the quantum wire case, where it was

found that mainly x-polarized photons attenuate the central system charging due to a closer agreement of the photon mode energy and the characteristic electronic excitation energy in x direction.[56] In this paper, we have considered a more complex geometry, which reduces effectively the y-confinement energy $\hbar\Omega_0 = 1.0$ meV. The characteristic electronic excitation energy in y direction may therefore be much closer to the photon mode energy $\hbar\omega = 0.4$ meV, thus leading to a relatively strong influence of the y-polarized photon field on the electronic transport. Transient spectroscopy has been applied to semiconductor microstructures.[63,64] We can only speculate that methods from quantum optics combined with methods developed for time-dependent electron transport can be used to make the time scale in our nanostructures accessible. The conceived magnetic field influenced quantum ring system in a photon cavity could serve as an elementary quantum device for optoelectronic applications and quantum information processing with unique characteristics by controlling the applied magnetic field and the polarization of the photon field.

ACKNOWLEDGMENTS

The authors acknowledge discussions of the manuscript with Olafur Jonasson. This work was financially supported by the Icelandic Research and Instruments Funds, the Research Fund of the University of Iceland, and the National Science Council of Taiwan under contract No. NSC100-2112-M-239-001-MY3.

*tla1@hi.is
†cstang@nuu.edu.tw
‡vidar@hi.is

[1] E. Buks, R. Schuster, M. Heiblum, D. Mahalu, and V. Umansky, Nature (London) **391**, 871 (1998).
[2] D. Sprinzak, E. Buks, M. Heiblum, and H. Shtrikman, Phys. Rev. Lett. **84**, 5820 (2000).
[3] A. Bertoni, P. Bordone, R. Brunetti, C. Jacoboni, and S. Reggiani, Phys. Rev. Lett. **84**, 5912 (2000).
[4] V. Gudmundsson and C.-S. Tang, Phys. Rev. B **74**, 125302 (2006).
[5] K. Kobayashi, H. Aikawa, A. Sano, S. Katsumoto, and Y. Iye, Phys. Rev. B **70**, 035319 (2004).
[6] O. Valsson, C.-S. Tang, and V. Gudmundsson, Phys. Rev. B **78**, 165318 (2008).
[7] B. Szafran and F. M. Peeters, Phys. Rev. B **72**, 165301 (2005).
[8] S. S. Buchholz, S. F. Fischer, U. Kunze, M. Bell, D. Reuter, and A. D. Wieck, Phys. Rev. B **82**, 045432 (2010).
[9] C. C. Eugster and J. A. del Alamo, Phys. Rev. Lett. **67**, 3586 (1991).
[10] D. M. Schroer, A. K. Huttel, K. Eberl, S. Ludwig, M. N. Kiselev, and B. L. Altshuler, Phys. Rev. B **74**, 233301 (2006).
[11] H.-F. Cheung, Y. Gefen, E. K. Riedel, and W.-H. Shih, Phys. Rev. B **37**, 6050 (1988).
[12] Y. Aharonov and D. Bohm, Phys. Rev. **115**, 485 (1959).
[13] M. Büttiker, Y. Imry, and M. Y. Azbel, Phys. Rev. A **30**, 1982 (1984).
[14] R. A. Webb, S. Washburn, C. P. Umbach, and R. B. Laibowitz, Phys. Rev. Lett. **54**, 2696 (1985).
[15] A. Tonomura, N. Osakabe, T. Matsuda, T. Kawasaki, J. Endo, S. Yano, and H. Yamada, Phys. Rev. Lett. **56**, 792 (1986).
[16] K. N. Pichugin and A. F. Sadreev, Phys Rev. B **56**, 9662 (1997).
[17] N. Byers and C. N. Yang, Phys. Rev. Lett. **7**, 46 (1961).
[18] S. Viefers, P. Koskinen, P. S. Deo, and M. Manninen, Phys. E **21**, 1 (2004).
[19] W.-C. Tan and J. C. Inkson, Phys. Rev. B **60**, 5626 (1999).
[20] T. Arnold, M. Siegmund, and O. Pankratov, J. Phys.: Condens. Matter **23**, 335601 (2011).
[21] W.-C. Tan and J. C. Inkson, Semicond. Sci. Technol. **11**, 1635 (1996).
[22] A. Fuhrer, P. Brusheim, T. Ihn, M. Sigrist, K. Ensslin, W. Wegscheider, and M. Bichler, Phys. Rev. B **73**, 205326 (2006).
[23] C. S. Tang and C. S. Chu, Phys. Rev. B **53**, 4838 (1996).
[24] M. A. Zeb, K. Sabeeh, and M. Tahir, Phys. Rev B **78**, 165420 (2008).
[25] D. Kienle and F. Léonard, Phys. Rev. Lett. **103**, 026601 (2009).
[26] C.-S. Tang, K. Torfason, and V. Gudmundsson, Comput. Phys. Commun. **182**, 65 (2011).
[27] C. S. Tang and C. S. Chu, Phys. Rev. B **60**, 1830 (1999).
[28] G. Zhou and Y. Li, J. Phys.: Condens. Matter **17**, 6663 (2005).
[29] J.-W. Jung, K. Na, and L. E. Reichl, Phys. Rev. A **85**, 023420 (2012).
[30] C. S. Tang and C. S. Chu, Physica B **292**, 127 (2000).
[31] G. Zhou, M. Yang, X. Xiao, and Y. Li, Phys. Rev. B **68**, 155309 (2003).
[32] P. Myöhänen, A. Stan, G. Stefanucci, and R. van Leeuwen, Phys. Rev. B **80**, 115107 (2009).
[33] G. Stefanucci, E. Perfetto, and M. Cini, Phys. Rev. B **81**, 115446 (2010).
[34] M. Tahir and A. MacKinnon, Phys. Rev. B **81**, 195444 (2010).
[35] P.-W. Chen, C.-C. Jian, and H.-S. Goan, Phys. Rev. B **83**, 115439 (2011).
[36] S. A. Gurvitz and Y. S. Prager, Phys. Rev. B **53**, 15932 (1996).
[37] N. G. van Kampen, *Stochastic Processes in Physics and Chemistry*, 2nd ed. (North-Holland, Amsterdam, 2001).
[38] U. Harbola, M. Esposito, and S. Mukamel, Phys. Rev. B **74**, 235309 (2006).
[39] A. Braggio, J. König, and R. Fazio, Phys. Rev. Lett. **96**, 026805 (2006).
[40] C. Emary, D. Marcos, R. Aguado, and T. Brandes, Phys. Rev. B **76**, 161404(R) (2007).
[41] A. Bednorz and W. Belzig, Phys. Rev. Lett. **101**, 206803 (2008).
[42] V. Moldoveanu, A. Manolescu, and V. Gudmundsson, New J. Phys. **11**, 073019 (2009).
[43] V. Gudmundsson, C. Gainar, C.-S. Tang, V. Moldoveanu, and A. Manolescu, New J. Phys. **11**, 113007 (2009).
[44] V. Gudmundsson, C.-S. Tang, O. Jonasson, V. Moldoveanu, and A. Manolescu, Phys. Rev. B **81**, 205319 (2010).
[45] M. Helm, *Intersubband Transitions in Quantum Wells: Physics and Device Applications I*, edited by H. C. Liu and F. Capasso (Academic Press, San Diego, CA, 2000).
[46] A. Gabbay, J. Reno, J. R. Wendt, A. Gin, M. C. Wanke, M. B. Sinclair, E. Shaner, and I. Brener, Appl. Phys. Lett. **98**, 203103 (2011).

[47]C. Ciuti, G. Bastard, and I. Carusotto, Phys. Rev. B **72**, 115303 (2005).
[48]M. Devoret, S. Girvin, and R. Schoelkopf, Ann. Phys. **16**, 767 (2007).
[49]A. A. Abdumalikov, O. Astafiev, Y. Nakamura, Y. A. Pashkin, and J. S. Tsai, Phys. Rev. B **78**, 180502(R) (2008).
[50]F. D. Zela, E. Solano, and A. Gago, Opt. Commun. **142**, 106 (1997).
[51]A. T. Sornborger, A. N. Cleland, and M. R. Geller, Phys. Rev. A **70**, 052315 (2004).
[52]E. K. Irish, Phys. Rev. Lett. **99**, 173601 (2007).
[53]E. B. Davies, *Quantum Theory of Open Systems* (Academic, London, 1976).
[54]H. Spohn, Rev. Mod. Phys. **52**, 569 (1980).
[55]H.-P. Breuer, B. Kappler, and F. Petruccione, Phys. Rev. A **59**, 1633 (1999).
[56]V. Gudmundsson, O. Jonasson, C.-S. Tang, H.-S. Goan, and A. Manolescu, Phys. Rev. B **85**, 075306 (2012).
[57]S. Nakajima, Prog. Theor. Phys. **20**, 948 (1958).
[58]R. Zwanzig, J. Chem. Phys. **33**, 1338 (1960).
[59]V. Gudmundsson, C. Gainar, C.-S. Tang, V. Moldoveanu, and A. Manolescu, New J. Phys. **11**, 113007 (2009).
[60]V. Moldoveanu, A. Manolescu, C.-S. Tang, and V. Gudmundsson, Phys. Rev. B **81**, 155442 (2010).
[61]R. S. Whitney, J. Phys. A: Math. Theor. **41**, 175304 (2008).
[62]V. Moldoveanu, A. Manolescu, and V. Gudmundsson, New J. Phys. **11**, 073019 (2009).
[63]W.-T. Lai, D. M. Kuo, and P.-W. Li, Phys. E **41**, 886 (2009).
[64]B. Naser, D. K. Ferry, J. Heeren, J. L. Reno, and J. P. Bird, Appl. Phys. Lett. **89**, 083103 (2006).